

Active lateral support system for a thin 1-meter meniscus mirror with virtual fixed points

Christian Schwaer^{a,*}, Andreas Sinn^a, Lukas Schroeer^a, Tobias Wallner^a, Georg Schitter^a

^aAutomation and Control Institute (ACIN), TU Wien, Gusshausstrasse 27-29, 1040 Vienna, Austria

Abstract.

This publication presents an active lateral support system for the thin 1-meter meniscus mirror of a Ritchey-Chrétien telescope system. The goal is to keep the mirror at its position under varying external influences, such as gravity and temperature, therefore maintaining the alignment and optical image quality. To achieve this, the lateral support consists of 8 actuators, based on stepper motors with gearboxes, with local force measurement and three laser triangulation sensors to measure the mirror's lateral position. A cascaded control structure with local force feedback in the inner loop and position feedback in the outer loop is proposed. In the outer loop, three SISO PI-controllers are implemented to maintain mirror position in the three lateral degrees of freedom (DOFs). The developed system is able to position the mirror with RMS errors of $0.27\ \mu\text{m}$ and $0.18\ \mu\text{m}$ in translational directions and $5.1\ \mu\text{rad}$ in the rotational direction over the operational altitude range with a slewing speed of $0.2\ \text{deg/s}$.

Keywords: active optics, telescopes, mirrors, mechatronic system design, control.

*Christian Schwaer, schwaer@acin.tuwien.ac.at

1 Introduction

Apart from utilization in the astronomical field, medium-sized telescope systems in the range of 0.4 m to 1.5 m have become increasingly popular in upcoming research fields such as satellite communication¹ or observation of space debris.² Considering deep-space communication,³ detection of small debris particles⁴ and the need for optical ground station networks (OGSNs),⁵ the utilized telescope systems require large apertures, robustness with respect to environmental influences, high optical quality and lightweight design for transportability and cost-effectiveness. For larger telescopes in astronomical applications with high requirements regarding imaging quality, a concept called active optics was developed in the 1980s and first implemented in the New Technology Telescope (NTT) of the European Southern Observatory (ESO),⁶ where actuators at the telescope mirrors control their shape and position. Since its invention, active optics systems were implemented in telescopes of varying sizes from 2.6 m to 8.0 m due to following advantages: the optical tolerances are eased, thinner and more flexible mirrors are possible, the thermal time constant is reduced, the maintenance and alignment is simplified and new mirror materials can be considered.⁶ This advantages also hold for smaller mirrors, however, as of now only few telescopes with diameters below 4.0 m utilize active optics.⁷ Implementing an active optics system in a medium-sized telescope with careful adaption of the actuation and sensing principles to smaller telescopes and different applications, such as space debris observation or optical satellite communication, promises to fulfill aforementioned requirements.⁷

In general, the active support system for meniscus mirrors is separated into two subsystems, the lateral support and the axial support. Meniscus mirrors combine the benefits of lightweight design with easy manufacturability compared to structured mirrors, and are therefore well suited for mentioned applications. While the axial support is used to control the mirror position in z -direction along the optical axis, the tip/tilt modes and the mirror shape, the lateral support deals

with controlling the mirror position in the xy -plane. This paper is focussed on the lateral support system only.

The first active optics system was put in operation in the 3.6 m NTT and revolutionized the field of astronomical telescopes. However, an active lateral support of the primary mirror was not considered for the 3.6 m mirror or its equivalent 1.0 m experimental mirror.^{6,8,9} This changed with the successors of the NTT which used the principle of active optics to build even larger telescopes with meniscus mirrors. The 8.2 m Very Large Telescope (VLT), like the NTT a project of the ESO, utilizes the beneficial Schwesinger-distribution of lateral forces.^{10,11} The lateral support consists of 64 passive hydraulic supports in push-pull arrangement. The pulling and pushing set of pads corresponding to each half of the mirror are hydraulically connected, thus acting as two virtual fixed points. The mirror's lateral position can be adjusted by controlling the volume of oil in each of the two hydraulic circuits.¹² A very similar concept with hydraulic whiffletrees and three lateral hydraulic zones is applied in the 8.0 m Gemini Telescope.¹³ The 8.2 m Subaru telescope utilizes a concept where electromechanical axial actuators protrude into the mirror through holes in its back with a counterweight placed at the end of a lever, thus also acting as passive lateral supports.¹⁴ This kind of structure with counterweights is also applied in the 2.6 m VLT Survey Telescope (VST) with 12 push and 12 pull supports, however, independent of the axial support.¹⁵

There are also systems that utilize an active lateral support system. In the 4.1 m Visible and Infrared Survey Telescope for Astronomy (VISTA) and the 4.2 m Daniel K. Inouye Solar Telescope (DKIST), formerly known as Advanced Technology Solar Telescope (ATST), the lateral support consists of 24 pneumatic cylinders.^{16,17} The 4.3 m Discovery Channel Telescope (DCT) and the 4.0 m Eastern Anatolia Observatory (DAG) also use double-acting pneumatic cylinders based on Schwesinger design with 36 and 24 supports, respectively.^{18,19} These active lateral systems are designed to have a force measurement at each of the actuators, thus enabling force control at every support point which consequently leads to increased optical performance.

However, with lateral actuators controlled only in force, the xy -position of the mirror as well as its rotation about the optical axis is not fixed. For this reason, lateral definers are implemented. The DAG has three mechanical lateral definers that set the lateral position of the mirror and its orientation around the optical axis.¹⁹ In the VST, three fixed points are arranged tangentially to the outer edge in order to preserve the mirror from stresses due to free thermal deformations of its cell, with load cells monitoring the delivered forces.¹⁵ The same concept is applied in the DCT and VISTA where each of the definers includes a precision length-adjustment screw to allow precise manual alignment.^{16,18} The primary mirror's lateral position in the VST and the VISTA is measured by two and three linear variable displacement transducers (LVDTs), respectively. This position is used in open-loop in case of the VISTA. In the DCT, the lateral definers are equipped with load cells to monitor the forces and use it a feedback loop to control the pressure in the pneumatic cylinders.¹⁸ In summary, the lateral definers are mechanical links that have to be adjusted manually which makes them tedious to assemble and maintain. Furthermore, the targeted applications introduce new requirements on the active optics system, especially regarding temperature influences. Mechanical links exert forces on the mirror when the mirror cell expands or contracts with respect to the mirror due to temperature changes, degrading the optical performance. For this reason, a contactless measurement for utilization in closed-loop control is proposed.

The contribution of this paper is the detailed analysis and experimental validation of a lateral support system for a thin meniscus mirror using electromechanical actuators and virtual fixed

points by means of optical metrology and feedback control. The utilization of electromechanical actuators based on stepper motors ensures the adaptability of the lateral forces under all circumstances, when compared to the passive, astatic system. This actuator type also prevents the necessity of additional large and heavy hardware such as compressors and hoses. Laser triangulation sensors provide non-contact position feedback of the mirror with respect to the mirror cell. With the proposed system the telescope should be able to be operated under varying temperature influences since the thermal expansion of the mirror cell or the mirror itself is not restricted by mechanical fixed points, thus no additional force with negative influence on the mirror surface shape is applied by the fixed points. Also, the necessity of aligning the mechanical fixed points manually is mitigated, consequently increasing telescope autonomy.

The paper is organized as follows. Section 2 provides a description of the laboratory setup including the utilized actuators and sensors. The error budget of the primary mirror system, i.e. the mirror including its support structure, is outlined in Section 3. Section 4 presents the system identification and control of the actuators and the complete support. In Section 5 the test results of the controlled system are provided. Finally, the conclusion and outlook are outlined in Section 6.

2 System Description

The primary mirror which is planned to be manufactured of borosilicate glass is replaced by an aluminum mirror for testing since aluminum has similar mechanical properties compared to borosilicate glass, see Table 1, but is easier to manufacture, less sensitive with respect to shocks and scratches and therefore better suited for testing in the laboratory during the development of the active optics system. The mirror geometry is outlined in Schwaer et al. 2020.⁷ Due to the lower mass of a glass mirror with equal geometry, the forces the lateral support system needs to take are larger with the aluminum mirror, which is considered insignificant for the purpose of this paper.

The aluminum mirror with its lateral support is embedded in a mirror cell that is rotatable in the altitude axis, see Fig. 1. The number of actuators as well as their placement were derived by a finite element (FE) analysis where the mirror was pointed to horizon. With the requirement of 17 nm RMS error, 51 nm peak-valley (PV) error and considering the yield strength of borosilicate glass, the number of actuators are obtained to eight.⁷ As mentioned in Section 1, electromechanical actuators are chosen due to their benefits. They are evenly distributed around the outer mirror edge and are oriented such that 70.4% of the total support force is applied tangentially and 29.6% radially.⁷ Since the mirror can not be supported at its center of gravity due to the meniscus shape, the lateral forces have components parallel to the optical axis in cosine distribution counted from the x -axis. The forces of the lateral actuators in Schwesinger-distribution have to be optimized for minimal mirror surface deformation in the real system, since effects such as manufacturing

Table 1: Material parameters of borosilicate glass and aluminum.

Parameter	Symbol	Glass	Aluminum	Unit
Density	ρ	2.23	2.7	$\text{g} \cdot \text{cm}^{-3}$
Young's modulus	E	63	68	GPa
Thermal expansion	α	$3.3 \cdot 10^{-6}$	$23 \cdot 10^{-6}$	K^{-1}
Poisson's ratio	ν	0.20	0.32	—
Mass	m	40.353	48.5	kg

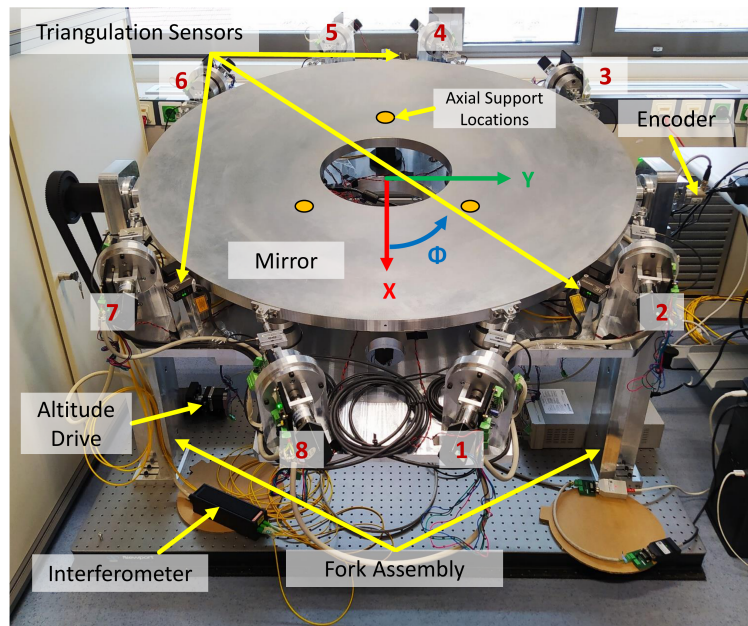


Fig 1: Complete system mounted on an optical breadboard. The aluminum mirror is supported by 8 lateral actuators, labeled from 1 to 8, and 3 axial fixed points. The position of the laser triangulation sensors is also shown. Due to the fork assembly, the mirror cell is rotatable about the altitude axis by the tooth belt drive.

and assembly tolerances might change the optimal force distribution compared to the one obtained by simulation. These optimal forces are determined by calibration, consisting of measuring the

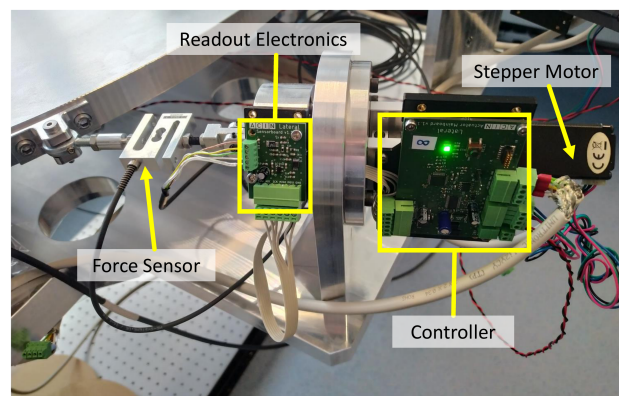


Fig 2: Detail view on the lateral actuator with its subsystems.

wavefront and optimizing the forces to minimize wavefront error over the angular, and possibly thermal, operating range of the telescope.

The actuator is based on a stepper motor with gearbox and 27:1 gear ratio. The translational movement is achieved by a trapezoidal screw with according nut. The link to the mirror consists of a flex pivot bearing, a force sensor and a ball joint as shown in Fig. 2. The commercial force sensor KD40s with ± 100 N nominal force from ME Messsysteme is based on strain gauges. On the sensor board, the signal is amplified and acquired by an analog-to-digital converter (ADC) which has a SPI connection to the main board where the data is processed by a STM32 microcontroller.

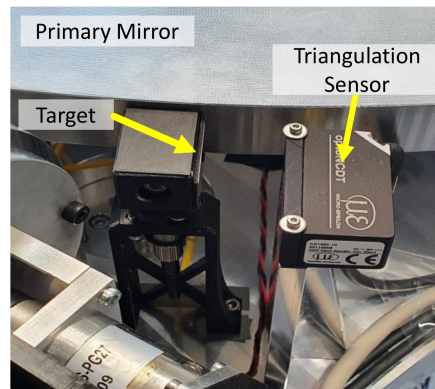


Fig 3: One of three triangulation sensors, attached to the mirror cell. Also shown is the target attached to the primary mirror.

Three optoNCDT 1320 laser triangulation sensors from Micro-Epsilon are placed in the xy -plane to measure the position of the mirror in x and y direction as well as the rotation about the z -axis, see Fig. 3. With their measuring range of 10 mm and repeatability below $1 \mu\text{m}$, they provide sufficient precision and range for all targeted applications. Also, due to their small size, they can be easily integrated into the mirror cell. All three sensors are connected to a shared microcontroller for data acquisition.

Every actuator microcontroller as well as the microcontroller for the triangulation sensors are separate nodes on a CAN bus system. The data of the triangulation sensors is sent to the host computer with a frequency of 50 Hz. The connection between the physical bus and the host is provided by a PCAN-USB device from PEAK System. For system controlling, data processing and feedback controller implementation, a software application is created using Python 3.10.

3 Error Budgeting

In order to determine if the proposed system is sufficient to fulfill the imposed requirements, an error budget analysis for the complete system, i.e. the primary mirror and the support structure, is carried out. The allowable RMS wavefront error for the primary mirror system is determined using the Strehl ratio St in the weak aberration limit,²⁰ defined as

$$St = \frac{I(S)}{I_0} \approx 1 - \left(\frac{2\pi}{\lambda} \right)^2 (W_{\text{RMS}})^2, \quad (1)$$

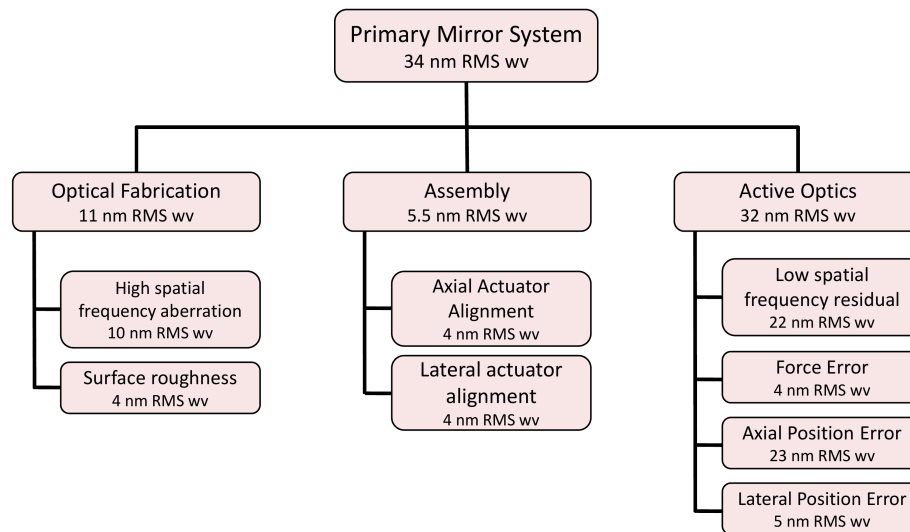


Fig 4: Overview of several contributors to total error budget.

where $I(S)$ is the peak intensity of the point spread function of the aberrated system, I_0 the one of the unaberrated system, λ the wavelength and W_{RMS} is the RMS wavefront error. Since the telescope system is required to achieve diffraction-limited performance, the Strehl ratio needs to be larger than 0.8.²¹ The primary mirror system alone, i.e. without considering other optical elements which might contribute to image degradation such as the secondary mirror, has to exceed this value. Therefore, a Strehl ration of 0.85 is awarded to the primary mirror, which equates to an allowed RMS wavefront error of 34 nm. A further main contributor to wavefront aberration is the secondary mirror which is planned to be active and positioned relative to the primary by means of optical metrology.²²

An overview of the total error budget with its lower-level contributors is shown in Fig. 4.

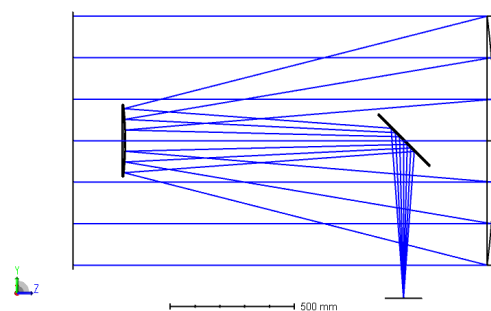


Fig 5: Telescope model used in Zemax OpticStudio 21.3.

Table 2: Optical parameters of the telescope system.

Parameter	Symbol	Primary	Secondary	Tertiary	Unit
Radius of curvature	R	4000	1445.885	inf	mm
Conic constant	K	-1.0586	-3.9753	0	–
Diameter	d	1000	290	294	mm
Distance	s	1700	-1488.1356	1120	–

Besides errors due to the optical fabrication and the assembly, the active optics system itself also contributes to the total surface error. A budget of 5 nm is awarded to the lateral position error which is used to derive the maximum permitted lateral displacement. Since Ritchey-Chrétien (RC) telescope systems are more sensitive to tilt than to lateral misalignment²³, more budget is awarded to the axial positioning. An analysis of the figure error is outlined in Schwaer et al. 2020.⁷

The RMS wavefront error of 5 nm introduced by lateral displacement is investigated by using Zemax OpticStudio 21.3. The telescope is a RC with a focal ratio of f6.85, primary mirror diameter of 1 m and Nasmyth focus, see Fig. 5. The optical parameters for the telescope are shown in Table 2. The distance parameter is thereby the distance of the optical element relative to its preceding element counted along the z -axis shown in Fig. 5.

Using Eq. (1), the Strehl ratio of the misaligned system calculates to 0.996 which equates to a decenter of around 10 μm of the primary mirror into one direction (x or y). The point spread function (PSF) of the aligned system as well as the PSF with the primary mirror displaced by this distance in y -direction is displayed in Fig. 6. The depicted center coordinates of the PSF make it clear that not only the peak intensity decreases, but also a shift of the PSF occurs due to the primary mirror displacement.

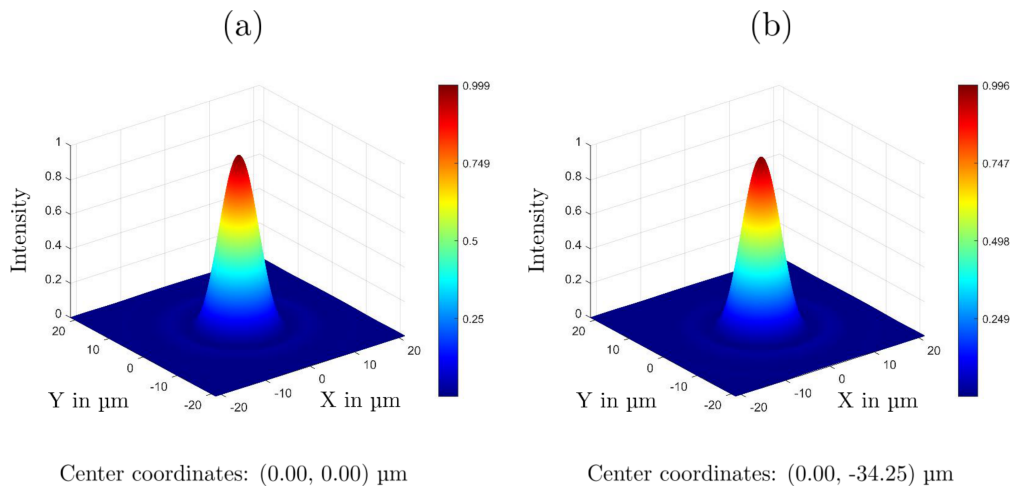


Fig 6: (a) Huygens PSF of the aligned system. (b) Huygens PSF with the primary mirror decentered by 10 μm in y -direction, leading to a 0.3% decrease of peak intensity. The PSF is centered in the plot by $-34.25 \mu\text{m}$.

4 System Identification and Control

In order to position the mirror within the $10\ \mu\text{m}$ maximum displacement in either x or y -direction, which is equivalent to $7.1\ \mu\text{m}$ when the mirror is displaced equally in both directions, a cascaded feedback loop is proposed. It consists of an inner loop with force feedback at every actuator and an outer loop that uses the data provided by position sensors to update the reference force values for the actuators, both axial and lateral, as shown in Fig. 7. In the following, only the lateral system with the triangulation sensors is considered.

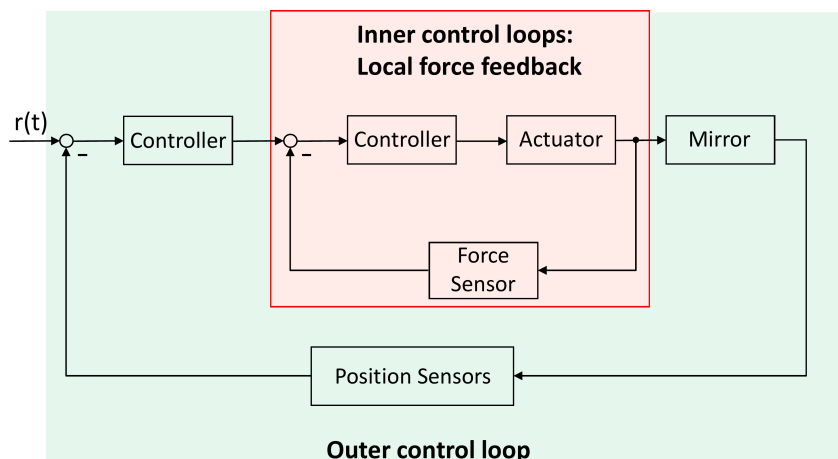


Fig 7: Block diagram of the cascaded control structure for both, the lateral and axial support system.

First, one lateral actuator is identified in order to design the proportional-integral (PI) controller with anti-windup (clamping) for its force feedback loop. In order to protect the mirror from damage, a force limit with automatic controller shut-off is implemented into the software. Second, the designed controller is implemented on all actuators and their complementary sensitivity function is measured at 75° altitude. The result can be seen in Fig. 8. Due to large manufacturing tolerances of the stepper motors (coil resistance and inductance) and gearboxes (backlash), a variation of the achievable closed-loop bandwidth is observed. However, these differences are of no concern since the control bandwidth of the outer positional loop is below the bandwidth of the actuators where the closed-loop differences are marginal. In general, the actuators show good reference tracking and the bandwidth of the slowest actuator (number 3) is around 3 Hz. Furthermore, the behavior of the actuators is independent of the altitude angle, i.e. the magnitude of the applied force has no influence on the actuators.

In order to position the mirror in lateral direction, the symmetry of the actuation is utilized. For example, a displacement in positive y -direction is achieved by increasing the force set points of actuators 1 to 4 while simultaneously decreasing them at actuators 5 to 8. This means, the sign of the force change is separated by the xz -plane. For a movement in x -direction, it is the yz -plane. A rotation about the optical axis is achieved by increasing and decreasing the force set points of diagonally placed actuators.

To derive the control strategy and parameters, the system behavior of the plant (force input to displacement output) is recorded for the three DOFs, i.e. a movement in one axis is excited by applying according forces at the actuators and the displacement in this axis as well as the crosstalk to all other axes is measured. This is done at three different zenith angles (15° , 45° , 70°) where $\Theta_{zenith} = 90^\circ - \Theta_{altitude}$, to investigate angle-dependent differences. With one exception at large angle, the crosstalks for the important x and y axes range from -10 dB to -30 dB, which justifies the utilization of individual SISO PI-controllers for these axes. The control parameters for the x -controller are $k_p = 1.0 \cdot 10^5$, $k_i = 2.5 \cdot 10^5$ and for the y -controller $k_p = 2.5 \cdot 10^5$, $k_i = 8.5 \cdot 10^5$. Taking into consideration that a rotation about the optical axis does not degrade the optical performance, however a slow drift has to be mitigated since the actuators would reach their end of range, a SISO PI-controller with much smaller bandwidth is implemented for Φ also.

After controller implementation, the sensitivity functions of the x and y axis are measured, demonstrating the disturbance rejection up to the sensitivity crossover frequency of 0.8 Hz in x and 1.3 Hz in y , as depicted in Figs. 9(a) and 9(c). When the sensitivity function in closed-loop for one axis is recorded, the influence on the other, uncontrolled axis is measured. The crosstalk from closed-loop x to open-loop y is shown in Fig. 9(b), the one from closed-loop y to open-loop x in Fig. 9(d). It is obvious that the crosstalk from x to y is acceptable with a magnitude of -10 to -30 dB. In the other direction, the crosstalk tends to increase with increasing angle, reaching around -4.5 dB for 70° . However, since both axes are going to be operated in closed-loop, the crosstalk acts as a disturbance from one to the other axis which is shown to be rejected by the controller.

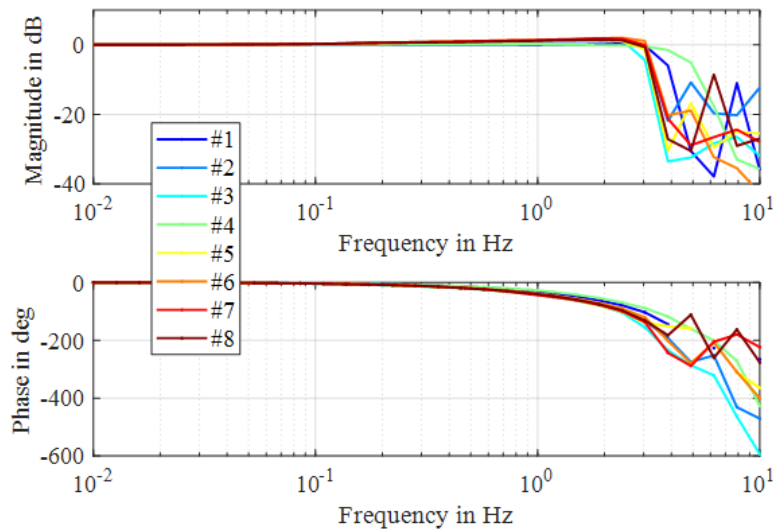


Fig 8: Complementary sensitivity function of all eight lateral actuators in force feedback control at 75° altitude (inner control loops).

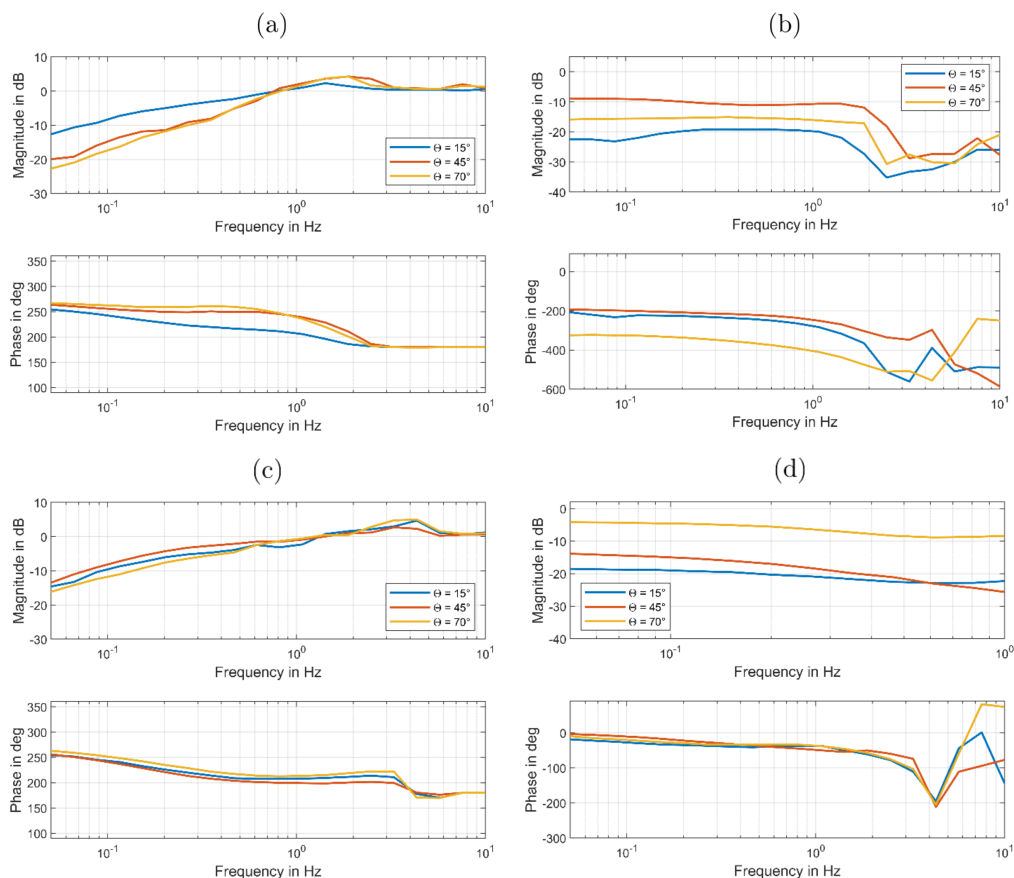


Fig 9: Bode plots of the outer loop with feedback control. (a) Sensitivity functions in x -direction. (b) Crosstalk from controlled x -axis to y . (c) Sensitivity functions in y -direction. (d) Crosstalk from controlled y -axis to x .

5 Results and Discussion

In order to evaluate the feasibility of the virtual fixed points by means of optical metrology with the proposed feedback control, the performance of the system with respect to resulting lateral displacement and necessary forces due to changing altitude angle is investigated. In this test case, the altitude angle can be seen as the disturbance to the system. The angle over time is shown in Fig. 10(a) with a gradient of 0.2 deg/s. This is already a speed as seen in more dynamic applications such as space debris observation and therefore poses a good challenge for the system.

The resulting displacements without control are shown as dashed lines, with control as solid lines in Fig. 10(b). It is obvious that without control especially the displacement in x gets quite large with a maximum of 241 μm and a RMS error of 140 μm with increasing angle since the gravity vector coincides with the x -axis when the mirror is pointing to horizon. However, the error in y is also significant with maximum displacement of $-101 \mu\text{m}$ and 53 μm RMS. The RMS

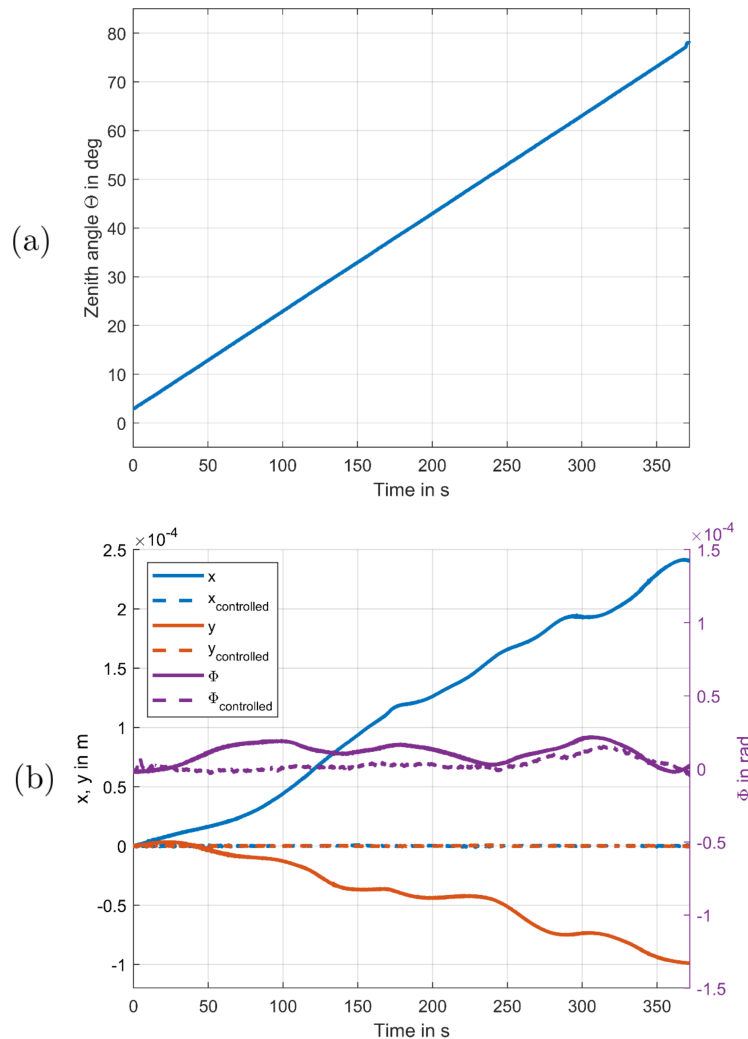


Fig 10: (a) Zenith angle over time which acts as the disturbance to the system. (b) Displacement resulting from the disturbance with and without control.

error of the angle Φ is $12.6 \mu\text{rad}$. With control, the RMS errors are reduced to $0.27 \mu\text{m}$ in x , $0.18 \mu\text{m}$ in y and $5.1 \mu\text{rad}$ in Φ which corresponds to an improvement of factor 519, 294 and 2.5, respectively. The maximum displacements of the controlled system are $1.23 \mu\text{m}$, $0.83 \mu\text{m}$ and $15.3 \mu\text{rad}$ in x , y and Φ . The maximum magnitude of the combined x and y displacements is $1.4 \mu\text{m}$ with $0.33 \mu\text{m}$ RMS, i.e. the controlled lateral system meets the imposed requirement of a displacement magnitude which is less than $10 \mu\text{m}$ comfortably.

When investigating the obtained results, the following has to be considered. First, the three axial fixed points used as support in axial direction are much stiffer and have a lot of friction compared to the planned axial support with laterally very compliant axial actuators.²⁴ Therefore, the

forces applied to the mirror for moving it are large and would certainly deform the mirror surface. Since the main contribution of this paper is the introduction of virtual fixed points by means of optical metrology and feedback control, and the transition from axial fixed points to the designed axial support is merely an adaptation of control parameters or strategy, the exact forces are disregarded and investigated closely when the axial support is integrated. Second, the optimal lateral force distribution for every angle between zenith and horizon has to be investigated by minimizing the deformation introduced by the lateral support. From this, a look-up table can be created and the position controller only needs to apply small forces when non-repeatable errors change mirror position. Since it is not yet possible to measure mirror deformation, the optimal force distribution is unknown, which is why the position controller sets the forces given by the implemented control law of applying the forces evenly distributed, which is not the ideal distribution.¹⁰ However, arbitrary reference values and controller output distributions are possible with the proposed system, i.e. it can be easily adapted to minimize the influence on the mirror shape.

In summary, it is successfully shown that the developed system is able to position the mirror laterally with a RMS error of $0.33\ \mu\text{m}$, achieving a positioning with a factor 30 below the stated requirement of $10\ \mu\text{m}$ derived in Section 3.

6 Conclusion

In this paper, the lateral support system for a thin 1-m meniscus mirror with virtual fixed points is developed and investigated. The virtual fixed points consist of an optical measurement together with feedback control. The developed system demonstrates an improvement of the position RMS error over the altitude angle of factor 519 and 294 in both lateral directions, respectively, compared to the uncontrolled system. Due to the contactless position measurement, the alignment process is significantly simplified, and the complete system can be operated in varying temperature conditions without negatively impacting the mirror surface by arising forces due to different thermal expansion coefficients of mirror cell and mirror, as would be the case with mechanical fixed points. This is achieved by using commercial and cost-efficient laser triangulation sensors. It is also possible to implement this system in every telescope system, independent of mirror geometry and material.

Building on the obtained results, future work will focus on the implementation of the axial subsystem, providing the possibility to further analyze the lateral support system with respect to its influence on the mirror surface since the arising lateral forces due to the control of the lateral support system represent the ones of the real system. Also, a metrology system for the investigation of the ability of the axial support to deform the mirror in its elastic modes to compensate for higher-order aberrations will be investigated.

Disclosures

The authors declare that they have no known competing financial interests or personal relationships that could have appeared to influence the work reported in this paper.

Acknowledgments

The authors gratefully acknowledge the cooperation with ASA Astrosysteme GmbH and thank for their support and valuable expertise.

This work was funded by the Austrian research funding association (FFG) under the scope of the Austrian Space Applications Programme (ASAP), contract number 873711.

References

- 1 H. Kaushal and G. Kaddoum, “Optical communication in space: Challenges and mitigation techniques,” *IEEE Communications Surveys Tutorials* **19**, 57–96 (2017). [doi:10.1109/COMST.2016.2603518].
- 2 A. Potter, “Ground-based optical observations of orbital debris: A review,” *Advances in Space Research* **16**(11), 35 – 45 (1995). [doi:10.1016/0273-1177(95)98751-9].
- 3 H. Hemmati, A. Biswas, and I. B. Djordjevic, “Deep-space optical communications: Future perspectives and applications,” *Proceedings of the IEEE* **99**, 2020–2039 (2011). [doi:10.1109/JPROC.2011.2160609].
- 4 M. Laas-Bourez, S. Wailliez, F. Deleflie, *et al.*, “First astrometric observations of space debris with the MeO telescope,” *Advances in Space Research* **49**(3), 603–611 (2012).
- 5 C. Fuchs and F. Moll, “Ground station network optimization for space-to-ground optical communication links,” *IEEE/OSA Journal of Optical Communications and Networking* **7**(12), 1148–1159 (2015).
- 6 R. N. Wilson, F. Franza, and L. Noethe, “Active optics I. A system for optimizing the optical quality and reducing the costs of large telescopes,” *Journal of Modern Optics* **34**(4), 485–509 (1987).
- 7 C. Schwaer, A. Sinn, P. Keller, *et al.*, “Design methodology to develop an active optics system for a thin 1-m meniscus mirror,” *Journal of Astronomical Telescopes, Instruments, and Systems* **6**(4), 1 – 22 (2020). [doi:10.1117/1.JATIS.6.4.049002].
- 8 L. Noethe, F. Franza, P. Giordano, *et al.*, “Active optics: II. Results of an experiment with a thin 1 m test mirror,” *Journal of Modern Optics* **35**(9), 1427–1457 (1988).
- 9 R. N. Wilson, F. Franza, P. Giordano, *et al.*, “Active optics III . Final results with the 1 m test mirror and NTT 3.58 m primary in the workshop,” *Journal of Modern Optics* **36**(11), 1415–1425 (1989).
- 10 G. Schwesinger, “Lateral support of very large telescope mirrors by edge forces only,” *Journal of Modern Optics* **38**(8), 1507–1516 (1991). [doi:10.1080/09500349114551681].
- 11 G. Schwesinger, “Nondistorting lateral edge support of large telescope mirrors,” *Applied Optics* **33**(7), 1198–1202 (1994).
- 12 D. Enard, “The european southern observatory very large telescope,” *Journal of Optics* **22**, 33–50 (1991).
- 13 M. K. Cho and L. M. Stepp, “Effect of Gemini primary mirror position relative to the lateral support on mirror figure,” in *Optical Design, Materials, Fabrication, and Maintenance*, P. Dierickx, Ed., **4003**, 165 – 175, International Society for Optics and Photonics, SPIE (2000).
- 14 M. Iye, “Subaru telescope - history, active/adaptive optics, instruments, and scientific achievements-,” *Proceedings of the Japan Academy. Series B, Physical and Biological Sciences* **97**, 337 – 370 (2021).
- 15 P. Schipani, S. D’Orsi, L. Ferragina, *et al.*, “Active optics primary mirror support system for the 2.6m VST telescope,” *Appl. Opt.* **49**(8), 1234–1241 (2010).

16 W. Sutherland, J. Emerson, G. Dalton, *et al.*, “The Visible and Infrared Survey Telescope for Astronomy (VISTA): Design, Technical Overview and Performance,” *Astronomy & Astrophysics* **575** (2015). [doi:10.1051/0004-6361/201424973].

17 G. P. Lousberg, V. Moreau, J.-M. Schumacher, *et al.*, “Design and analysis of an active optics system for a 4-m telescope mirror combining hydraulic and pneumatic supports,” in *Optical Systems Design 2015: Optical Design and Engineering VI*, L. Mazuray, R. Wartmann, and A. P. Wood, Eds., **9626**, 962624, International Society for Optics and Photonics, SPIE (2015).

18 B. Smith, T. Chylek, B. Cuerden, *et al.*, “The Active Optics System for the Discovery Channel Telescope,” *Proc. SPIE* **7739**(63) (2010). [doi:10.1117/12.858047].

19 G. P. Lousberg, E. Mudry, C. Bastin, *et al.*, “Active optics system for the 4m telescope of the Eastern Anatolia Observatory (DAG),” *Proc. SPIE* **9912** (2016). [doi:10.1117/12.2234261].

20 M. Born and E. Wolf, *Principles of Optics*, Pergamon, 5 ed. (1975).

21 R. N. Wilson, *Reflecting Telescope Optics I*, Springer-Verlag Berlin Heidelberg (2007).

22 A. Sinn, P. Prager, C. Schwaer, *et al.*, “Design and evaluation of an active secondary mirror positioning system for a small telescope,” *Journal of Astronomical Telescopes, Instruments, and Systems* **8**(2), 029007 (2022).

23 D. J. Schroeder, *Astronomical Optics*, Academic Press, 2nd ed. (2000).

24 C. Schwaer, D. Stefanek, A. Sinn, *et al.*, “Integrated force sensor based on optical distance measurement for a modular actuator used in active optics,” in *2022 IEEE/ASME International Conference on Advanced Intelligent Mechatronics (AIM)*, 496–501 (2022).

Tables

Parameter	Symbol	Glass	Aluminum	Unit
Density	ρ	2.23	2.7	$\text{g} \cdot \text{cm}^{-3}$
Young’s modulus	E	63	68	GPa
Thermal expansion	α	$3.3 \cdot 10^{-6}$	$23 \cdot 10^{-6}$	K^{-1}
Poisson’s ratio	ν	0.20	0.32	–
Mass	m	40.353	48.5	kg

Parameter	Symbol	Primary	Secondary	Tertiary	Unit
Radius of curvature	R	4000	1445.885	inf	mm
Conic constant	K	-1.0586	-3.9753	0	–
Diameter	d	1000	290	294	mm
Distance	s	1700	-1488.1356	1120	–

List of Figures

1	Complete system mounted on an optical breadboard. The aluminum mirror is supported by 8 lateral actuators, labeled from 1 to 8, and 3 axial fixed points. The position of the laser triangulation sensors is also shown. Due to the fork assembly, the mirror cell is rotatable about the altitude axis by the tooth belt drive.	4
2	Detail view on the lateral actuator with its subsystems.	4
3	One of three triangulation sensors, attached to the mirror cell. Also shown is the target attached to the primary mirror.	5
4	Overview of several contributors to total error budget.	6

5	Telescope model used in Zemax OpticStudio 21.3.	6
6	(a) Huygens PSF of the aligned system. (b) Huygens PSF with the primary mirror decentered by $10\ \mu\text{m}$ in y -direction, leading to a 0.3% decrease of peak intensity. The PSF is centered in the plot by $-34.25\ \mu\text{m}$	7
7	Block diagram of the cascaded control structure for both, the lateral and axial support system.	8
8	Complementary sensitivity function of all eight lateral actuators in force feedback control at 75° altitude (inner control loops).	9
9	Bode plots of the outer loop with feedback control. (a) Sensitivity functions in x -direction. (b) Crosstalk from controlled x -axis to y . (c) Sensitivity functions in y -direction. (d) Crosstalk from controlled y -axis to x	10
10	(a) Zenith angle over time which acts as the disturbance to the system. (b) Displacement resulting from the disturbance with and without control.	11